Modeling of the Denebulization of Warm Fogs by Hygroscopic Seeding: Effect of Various Operating Conditions and of the Turbulence Intensity

Nicolas Reuge, Pascal Fede, Jean-François Berthoumieu, Florian Foucoin, Olivier Simonin

Modeling of the Denebulization of Warm Fogs by Hygroscopic Seeding: Effect of Various Operating Conditions and of the Turbulence Intensity

N. REUGE AND P. FEDE

Institut de Mécanique des Fluides de Toulouse, Université de Toulouse, CNRS, INPT, UPS, Toulouse, France

J.-F. BERTHOUMIEU

ACMG Agralis Services, Le Passage, France

F. FOUCOIN

Etienne Lacroix, Muret, France

O. SIMONIN

Institut de Mécanique des Fluides de Toulouse, Université de Toulouse, CNRS, INPT, UPS, Toulouse, France

(Manuscript received 14 April 2016, in final form 10 October 2016)

ABSTRACT

This study addresses the modeling of the denebulization (i.e., the removal of droplets) of warm fogs ($T \geq 0°C$) by hygroscopic salt microparticles from the initial seeding at the top of the fog layer to the fall of the rain droplets on the ground. Two main phenomena can occur: condensation of water vapor on salted droplets and the concomitant evaporation of fog droplets, and coalescence between the salted droplets and the fog droplets. Three salts have been investigated: NaCl, $CaCl_2$, and KCl. Based on the conservation equations, the modeling approach (1D) considers the hygroscopicity of the salts through the water activity in the aqueous solution and the coalescence induced by gravity and turbulence. From this study, NaCl is the most efficient salt in the tested operating conditions. Actually, this result can be explained by the strong hygroscopicity of this salt in very dilute solutions. From the calculations, 15 kg of NaCl particles of 6.7-μm diameter can dissipate a typical fog layer of 40 m in height within less than 17 min over 0.25 km^2. According to the calculations, a fog layer of 100 m in height can be denebulized within 45 min. The contribution of the coalescence induced by gravity and by turbulence seems to have a negligible effect on the final horizontal visibility, the condensation/evaporation phenomena being preponderant for these operating conditions.

1. Introduction

Coupled evaporation/condensation/coalescence phenomena of droplets combined with particles for seeding are involved in a wide range of various applications from the environmental fields—clouds and fogs (Jiusto et al. 1968) and air pollution (Van Hop 1989)—to some industrial processes: spray generation, spray drying, and spray mixing (Hinds 1982; Reuge et al. 2008).

Cloud or fog particle seeding is an old technique of rain enhancement that began in the 1940s. Various methods have been tested: the use of dry ice (Schaefer 1946), then seeding by silver iodide, and since the 1990s the use of hygroscopic flares allowing seeding with hygroscopic salts (NaCl, $CaCl_2$, KCl, etc.; Mather et al. 1997). Planes were used to carry the flares. Nowadays, they can be replaced by drones: the costs of this technique would be reduced very significantly. Indeed, a drone equipped with hygroscopic flares could be used for a local seeding over a very specific zone of a fog, by day or night. Therefore, in the present study, the efficiency of this technique is investigated regarding fog dissipation. Just after the seeding, these steps are expected: first, the condensation of water vapor on seed microparticles and concomitant deliquescence of these microparticles (this step is very fast, <1 s); then, the step of condensation of water vapor on salted droplets and

Corresponding author e-mail: N. Reuge, reuge@free.fr

DOI: 10.1175/JAMC-D-16-0151.1

the concomitant evaporation of fog or cloud water droplets; and, finally, the coalescence step when the diameter of the salted droplets is large enough. The efficiency of this technique is rather difficult to quantify: the huge variety of clouds/fogs and of their characteristics prevents us from testing the reproducibility. For this reason, modeling studies can be of great help.

The first modeling studies of this technique deal with the hygroscopic seeding of fogs (Jiusto et al. 1968; Kornfeld 1970; Silverman and Kunkel 1970; Koening 1971). The baseline work is the study of Silverman and Kunkel (1970). They use a 1D model in which monodispersed salt particles (NaCl) fall through a bidispersed fog layer, taking into account evaporation–condensation phenomena and coalescence induced by gravity. From their calculations, the technique seems really efficient, seeding the fog with reasonable NaCl quantities with appropriate seed particle diameters. The optimal initial particle diameter is around 10 μm, and the fog dissipation last for a few minutes. If the seed particle diameter is too small, the dissipation lasts too long, and the larger the seed diameter, the greater the quantity of NaCl required to dissipate the fog layer. Moreover, they have shown that this required salt quantity is proportional to the initial liquid water mass fraction in the fog layer. The same authors (Kunkel and Silverman 1970) have used the same model to compare the efficiency of different salts. According to their results, the most efficient salts are the hydroxides, followed by chlorides, bromides, nitrates, iodides, and finally sulfates.

Since the end of the 1990s, a few new modeling studies have been published regarding the hygroscopic seeding of clouds. They consider the cloud scale and are based on Eulerian–Lagrangian parcels 2D/3D computational fluid dynamics approaches. They take into account the convective flows into the clouds and the polydispersion of the particle/droplet sizes. The study of Cooper and Bruintjes (1997) shows that the presence of submicronic particles generated by the flares (mean diameter about 0.3 μm) has a negative impact on the denebulization process. The abundance of too-small particles/droplets is a drawback because they cannot reach sufficiently large diameters by condensation, and as a result coalescence phenomena cannot occur. From an initial particle diameter of 1 μm, the denebulization is efficient. Segal et al. (2004) performed the same kind of study emphasizing the importance of seeding with initial particles diameters greater than 2 μm. The lower the mass fraction of submicronic particles, the greater the efficiency of the technique. The optimal diameter lies between 3 and 5 μm, depending on the particle concentrations in the clouds. Finally, Kuba and Murakami's (2010) calculations proved the efficiency of the technique provided a sufficient amount of big particles is seeded. They also showed that the optimal diameter of seeded particles becomes larger with the increase in the total mass of seeded particles.

Therefore, from these modeling studies, it seems that artificial rains induced by seeding could be a really efficient technique. The optimal quantity and diameter of the salt particles to seed depend on various parameters such as the initial liquid mass fraction in the cloud/fog, the height of the layer, the convection and turbulence intensities, and the size distribution of the droplets. Only salt particle diameters greater than 1 μm seem interesting. The presence of submicronic particles seems to lower the technique efficiency. 1D modeling studies of the team of Silverman led to very interesting results that have been confirmed and completed by the 2D–3D models (Cooper and Bruintjes 1997; Segal et al. 2004; Kuba and Murakami 2010).

Our study focuses on fog denebulization by seeding, using sustainable materials. The targeted application that has motivated this work is to dissipate fog at an airport in an area extending between the control tower and the beginning of the runway over a height equal to the tower height.

Fogs are relatively homogeneous when compared with clouds, and therefore the use of a 1D approach seems pertinent. Different salts are considered and compared in terms of denebulization efficiency. The effects of the fog characteristics and of the initial seed particle diameter are studied. The effect of the presence of submicronic particles is investigated. Finally, the effect of the turbulence intensity on coalescence phenomena is examined.

2. Mathematical modeling

This section is set in the context of eight assumptions, labeled i–viii. (i) Gas and liquid phases have the same temperature, which is constant over time. (ii) The deliquescence step is very short (<1s) and is ignored in the model; the initial state of the salt particles is liquid. Two liquid phases k ($k = \alpha$ or β) are considered: α for the pure water phase (fog droplets) and β for the salted droplets phase. (iii) Fog and salted droplets diameters are greater than 1 μm, and therefore the Brownian motion is insignificant. (iv) Initial fog droplets and salt particles size distributions are assumed to be monodisperse. Thus, the balance equations for number densities take the following form:

$$\frac{\partial N_\alpha}{\partial t} = -\frac{\partial}{\partial z}(N_\alpha v_\alpha) - F_{\alpha\beta} \quad \text{and} \tag{1}$$

$$\frac{\partial N_\beta}{\partial t} = -\frac{\partial}{\partial z}(N_\beta v_\beta), \tag{2}$$

where N_k are the droplet number densities, $F_{\alpha\beta}$ is the coalescence frequency between fog and salted droplets, and v_k is the droplet terminal settling velocity. Note that inside a given class k, it is assumed that there is no coalescence.

(v) Then it is assumed that the Kelvin effect is negligible (diameters $> 0.1\,\mu$m). (vi) Convection and axial diffusion of air and water vapor are ignored. The mass balance equations are the following:

$$\frac{\partial}{\partial t}(\rho_w \varepsilon_\alpha) = -\frac{\partial}{\partial z}(\rho_w \varepsilon_\alpha v_\alpha) + \frac{3}{2}\varepsilon_\alpha \mathrm{Sh}_\alpha D_v M_w (RT r_\alpha^2)^{-1}(P_{\mathrm{vap}} - P_{\mathrm{sat}}) - \rho_w (4/3)\pi r_\alpha^3 F_{\alpha\beta} \quad \text{and} \tag{3}$$

$$\frac{\partial}{\partial t}(\rho_\beta \varepsilon_\beta) = -\frac{\partial}{\partial z}(\rho_\beta \varepsilon_\beta v_\beta) + \frac{3}{2}\varepsilon_\beta \mathrm{Sh}_\beta D_v M_w (RTR_\beta^2)^{-1}(P_{\mathrm{vap}} - P_s) + \rho_\beta (4/3)\pi r_\alpha^3 F_{\alpha\beta}, \tag{4}$$

where ρ_k are the densities, ε_k are the volume fractions, Sh_k are the Sherwood numbers, D_v is the diffusion coefficient of water vapor in air, M_k are the molar masses, r_α is the fog droplet radius, and R_β is the salted droplet radius. On right-hand side of Eqs. (3) and (4), the first terms represent the convection, the second terms represent the evaporation in Eq. (3) and the condensation in Eq. (4), and the third terms represent the coalescence.

(vii) For an initial salt particle radius $R_{\beta,0}$ with an initial density $\rho_{\beta,0}$, an initial radius $R'_{\beta,0} = R_{\beta,0}(\rho_{\beta,0}/\rho_w)^{1/3}$ is actually considered with a constant droplet density equal to ρ_w (the validity of this assumption has been confirmed by preliminary 0D calculations). Therefore, the mass balance equations are given by

$$\frac{\partial \varepsilon_\alpha}{\partial t} = -\frac{\partial}{\partial z}(\varepsilon_\alpha v_\alpha) + \frac{3}{2}\varepsilon_\alpha \mathrm{Sh}_\alpha D_v M_w (\rho_w RT r_\alpha^2)^{-1}(P_{\mathrm{vap}} - P_{\mathrm{sat}}) - (4/3)\pi r_\alpha^3 F_{\alpha\beta} \quad \text{and} \tag{5}$$

$$\frac{\partial \varepsilon_\beta}{\partial t} = -\frac{\partial}{\partial z}(\varepsilon_\beta v_\beta) + \frac{3}{2}\varepsilon_\beta \mathrm{Sh}_\beta D_v M_w (\rho_w RTR_\beta^2)^{-1}(P_{\mathrm{vap}} - P_s) + (4/3)\pi r_\alpha^3 F_{\alpha\beta}. \tag{6}$$

In a given volume, the total mass of water (liquid + vapor) changes are only due to convective fluxes. Thus, the mass balance equation for water (liquid + vapor) can be written as follows:

$$\frac{\partial \varepsilon_w}{\partial t} = -\frac{\partial}{\partial z}(\varepsilon_\alpha v_\alpha) - \frac{\partial}{\partial z}(\varepsilon_{w,\beta} v_\beta). \tag{7}$$

Finally, the water vapor partial pressure P_{vap} is given by

$$P_{\mathrm{vap}} = \rho_w RTM_w^{-1}(\varepsilon_w - N_\alpha \varepsilon_\alpha - N_\beta \varepsilon_{w,\beta}). \tag{8}$$

The water vapor partial pressure in air P_{sat} is calculated by the relation of Reid et al. (1977):

$$P_{\mathrm{sat}} = (10^5/760)\exp[18.3036 - 3816.44(T - 46.13)^{-1}]. \tag{9}$$

At the salted droplet surface, the saturation partial pressure of water vapor P_s is given by

$$P_s = a_{w,\beta} P_{\mathrm{sat}}. \tag{10}$$

The water activity in the solution $a_{w,\beta}$ varies with the nature of the salt and its concentration (see section 3a).

The coalescence frequency $F_{\alpha\beta}$ is given by

$$F_{\alpha\beta} = \pi \Gamma_{\alpha\beta} N_\alpha N_\beta (r_\alpha + R_\beta)^2 g_{r,\alpha\beta} E_{\mathrm{coll}}(r_\alpha, R_\beta) E_{\mathrm{coal}}(r_\alpha, R_\beta), \tag{11}$$

where $\Gamma_{\alpha\beta}$ is the radial distribution function (equal to 1 on condition of neglecting the preferential accumulation effect), $g_{r,\alpha\beta}$ is the mean relative velocity between droplets of phase α and droplets of phase β. The term E_{coll} is the collision efficiency, which is strongly dependent on r_α and R_β; it has been estimated using the data of Pinsky et al. (2001). The term E_{coal} is the coalescence efficiency; the model of Beard and Ochs (1995) has been considered. These references are much more recent and reliable that the ones used in the first modeling studies. The product of E_{coll} and E_{coal} is the collection efficiency: the obtained data are shown in Fig. 1 of Reuge et al. (2015).

Following studies on gas–particle turbulent flows (Kruis and Kusters 1997; Gourdel et al. 1999; Zaichik et al. 2009), the mean droplet–droplet relative velocity is given by

$$g_{r,\alpha\beta} = \sqrt{\frac{16}{\pi}\frac{2}{3}q_{r,\alpha\beta} + (v_\beta - v_\alpha)^2}. \tag{12}$$

In Eq. (12), the first term on the right-hand side is the contribution of the droplet–droplet relative agitation, and the second term is the contribution of the mean droplet–droplet relative impact velocity. As we consider only a 1D configuration, the mean droplet–droplet relative velocity is directly the difference between the terminal settling velocities of the droplets.

The relative agitation of the droplets is given by $q_{r,\alpha\beta}$, which can be written in terms of droplet kinetic energy (Pigeonneau 1998; Zaichik et al. 2009):

$$q_{r,\alpha\beta} = \frac{1}{2}\left(q_\alpha^2 + q_\beta^2 - 2\sqrt{q_\alpha^2 q_\beta^2 \zeta_\alpha \zeta_\beta}\right), \tag{13}$$

where q_α^2 and q_β^2 are the agitation of the droplets, and ζ_α and ζ_β are the gas–droplet correlation coefficients:

$$\zeta_\alpha = \frac{q_{f\alpha}}{2k}\frac{q_{f\alpha}}{2q_\alpha^2} \quad \text{and} \tag{14}$$

$$\zeta_\beta = \frac{q_{f\beta}}{2k}\frac{q_{f\beta}}{2q_\beta^2}, \tag{15}$$

where q_{fk} are the fluid–droplet covariances.

(viii) Assuming a homogeneous isotropic turbulence and that the droplets follow the Tchen and Hinze local equilibrium, then

$$2q_k^2 = q_{fk} = 2k\frac{\eta_{fk}}{1+\eta_{fk}}, \tag{16}$$

where $\eta_{fk} = \tau_f/\tau_{pk}$ is the inverse of the Stokes number, τ_f is the Lagrangian turbulent time scale, and $\tau_{pk} = \rho_k d_k^2/18\mu_a$ is the particle response time scale. Finally, the fog-droplet–salted-droplet relative velocity reads as follows:

$$\begin{aligned} q_{r,\alpha\beta} &= \frac{1}{2}\left(q_\alpha^2 + q_\beta^2 - 2k\frac{\eta_{t\alpha}}{1+\eta_{t\alpha}}\frac{\eta_{t\beta}}{1+\eta_{t\beta}}\right) \\ &= \frac{k}{2}\left(\frac{\eta_{t\alpha}}{1+\eta_{t\alpha}} + \frac{\eta_{t\beta}}{1+\eta_{t\beta}} - 2\frac{\eta_{t\alpha}}{1+\eta_{t\alpha}}\frac{\eta_{t\beta}}{1+\eta_{t\beta}}\right). \end{aligned} \tag{17}$$

The Lagrangian turbulent time scale may take into account the crossing trajectory effect (Yudine 1959; Csanady 1963); however, in the present modeling, this effect is neglected and such a time scale is computed with $\tau_f = k/\varepsilon$. Therefore, according to these expressions, coalescence induced by turbulence depends on both the turbulence kinetic energy k and the dissipation rate of the turbulence kinetic energy ε.

The droplets' terminal settling velocity has been estimated by the Stokes–Cunningham law (Cunningham 1910):

$$v_k(r) = C_c\frac{g(2r)^2(\rho_w - \rho_a)}{18\mu_a}, \quad \text{with} \tag{18}$$

$$C_c = 1 + \frac{2\lambda_m}{d}\left[1.257 + 0.4e^{-(1.1d/2\lambda_m)}\right]. \tag{19}$$

To prevent the occurrence of some numerical oscillations, combinations of Eqs. (1) and (5) and (2) and (6) have been used instead of Eqs. (3) and (4); these new equations clearly express the time derivatives of the droplets' radii:

$$\begin{aligned} \frac{\partial r_\alpha^3}{\partial t} &= -v_\alpha\frac{\partial r_\alpha^3}{\partial z} \\ &\quad + \frac{3}{2}r_\alpha \mathrm{Sh}_\alpha D_v M_w(\rho_w RT)^{-1}(P_{\mathrm{vap}} - P_{\mathrm{sat}}) \quad \text{and} \end{aligned} \tag{20}$$

$$\begin{aligned} \frac{\partial R_\beta^3}{\partial t} &= -v_\beta\frac{\partial R_\beta^3}{\partial z} \\ &\quad + \frac{3}{2}R_\beta \mathrm{Sh}_\beta D_v M_w(\rho_w RT)^{-1}(P_{\mathrm{vap}} - P_s) \\ &\quad + r_\alpha^3 N_\beta^{-1} F_{\alpha\beta}. \end{aligned} \tag{21}$$

The equations are solved by a coupling method, and the time integration is performed by an Euler scheme.

3. Application to the denebulization of a fog layer

As explained in the introduction, the model described in section 2 is applied to investigate the denebulization of a fog layer by hygroscopic particle seeding. In the present section, the material properties of such particles, along with the properties of the considered fog, are described.

a. Hygroscopic particle and fog material properties

The composition and the size distribution of the particles in the plumes generated by the flares seem to vary significantly depending on the manufacturer. They contain one hygroscopic salt or a mixture of different salts and some products of combustion in various proportions. In this study, the particles to be considered are composed of one given salt, and the products of combustion will be ignored. The size distributions are usually bimodal: a high proportion of the volume fraction is constituted of supermicronic particles with a peak in the range of 5–10 μm, and a high proportion of the number fraction is constituted of submicronic particles of about 100–300 nm. It seems that the formation of these submicronic particles cannot be prevented. Their effect on the denebulization process will be investigated.

In an aqueous solution, the hygroscopicity of a salt is directly linked with the water activity ($a_{w,\alpha}$). The water activity is defined as the ratio of the vapor pressure of water at the surface of an aqueous solution to the vapor pressure of pure water at the same temperature. The higher the hygroscopicity of the salt, the lower the water activity; note that pure water activity is 1. Herein, 15 different salts have been investigated. Water activities of solutions containing these salts in an ionic form are given by Hamer and Wu (1972) and Rard and Clegg (1997) and are shown in Fig. 1 as a

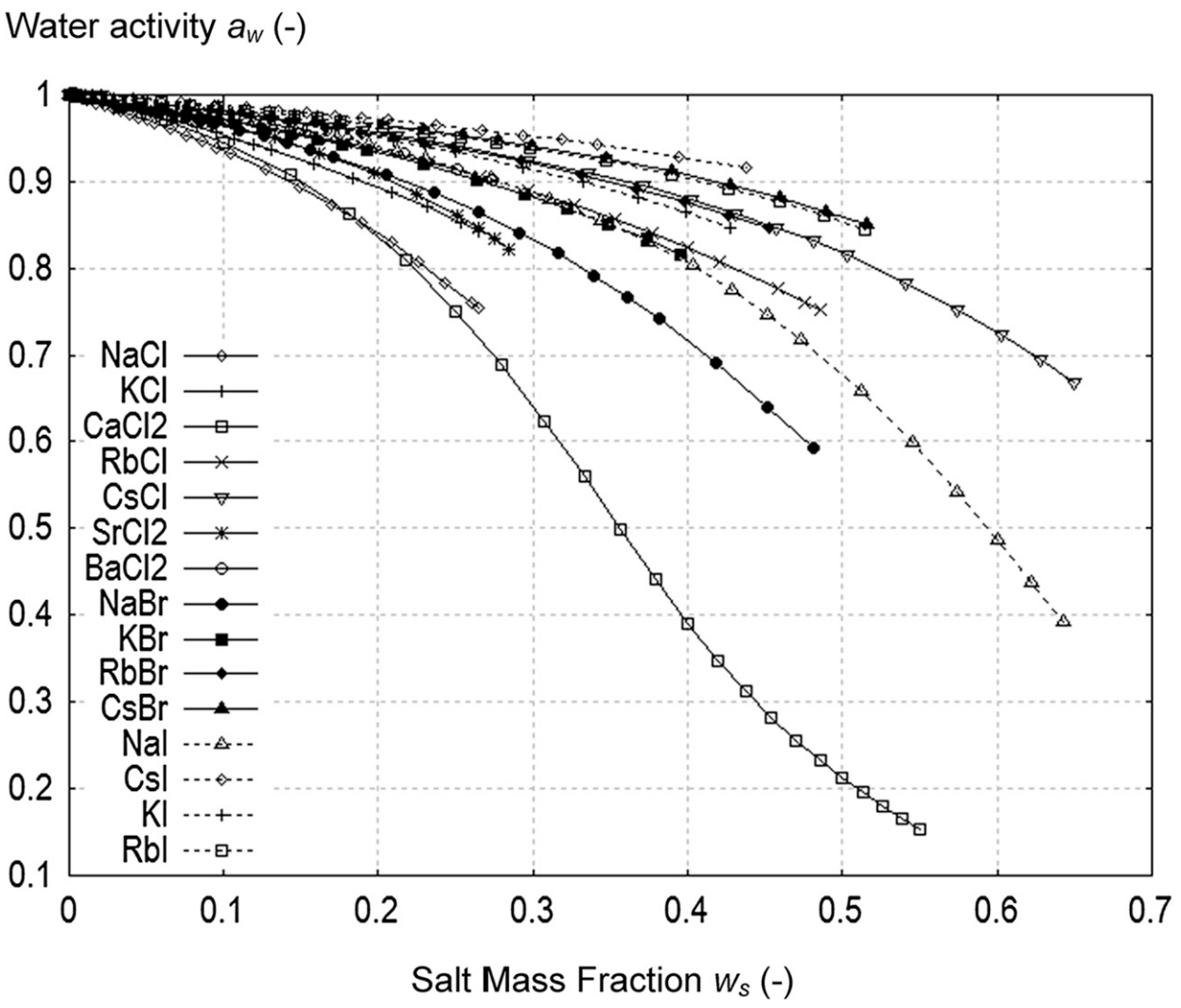

FIG. 1. Water activity in an aqueous solution as a function of the salt mass fraction w_s for various salts.

function of the salt mass fraction w_s. At low dilution rates, solutions containing $CaCl_2$ are the most hygroscopic (i.e., lowest water activity) but this is not the case at high dilution rates: for w_s lower than 0.18, solutions containing NaCl become the most hygroscopic, as shown in Fig. 2, and even solutions containing KCl are slightly more hygroscopic than solutions containing $CaCl_2$ for w_s lower than 0.025. Therefore, in this study we decided to test these three salts: $CaCl_2$, NaCl, and KCl.

By convention, a layer of droplets lying over the ground is called a fog when the horizontal visibility (HV) is lower than 1000 m. Typically, the liquid water content in fogs can vary between 0.05 and 0.5 $g.m^{-3}$ and the droplet number density can vary between 100 and 600 cm^{-3}. In fogs, air is saturated by water vapor; in other words, the relative humidity (RH) is 100%.

In clouds, the turbulence promotes the coalescence of the droplets and finally the formation of rain. In fog, wind and turbulence are much lower, which explains their stability (dissipation of fogs is mainly due to increases of wind and/or turbulence or temperature changes). From the few data available in the literature (Liu et al. 2011; Dupont et al. 2012; Han et al. 2015), typical values of k and ε in fogs are 0.1 and 10 $cm^2 s^{-3}$, respectively. In some valley fogs and in stratus, their values are about 1 and 100 $cm^2 s^{-3}$, respectively. Note that in particularly turbulent clouds, ε can reach 1000 $cm^2 s^{-3}$.

b. Numerical simulation overview

A typical warm fog has been considered with a fog droplet number density $N_{\alpha,0}$ profile showed in Fig. 3 and a droplet diameter $d_{\alpha,0}$ of 10 μm. Thus, the initial

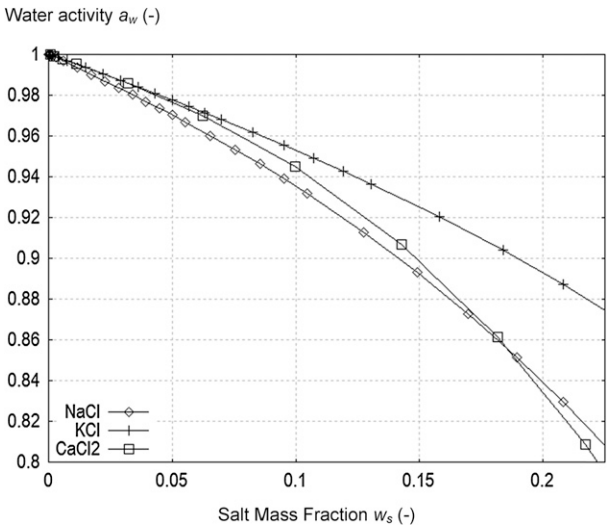

FIG. 2. Water activity in an aqueous solution as a function of the salt mass fraction w_s for NaCl, KCl, and $CaCl_2$.

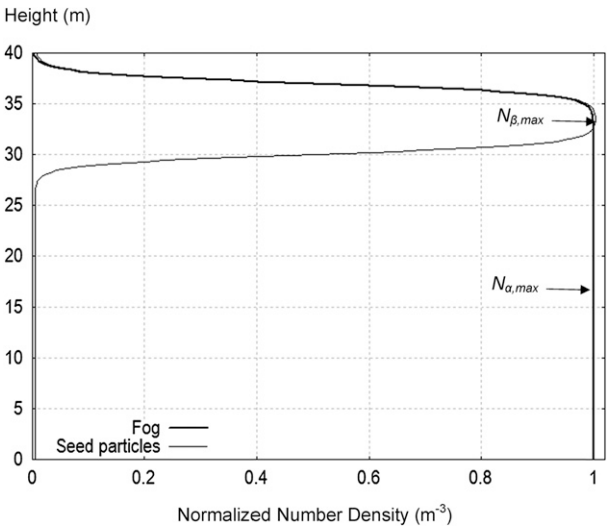

FIG. 3. Initial normalized number densities of fog droplets and seed particles vs height.

layer height H_0 is 40 m, but the horizontal visibility is lower than 1000 m over a 37-m height. A temperature of 10°C throughout the layer has been chosen. The initial RH is 100%. An initial diameter $d_{\beta,0}$ of 6.7 μm has been considered for the salt particles (i.e., a particle mass about 3.4×10^{-4} μg) initially seeded at the top of the fog layer according to the number density profile $N_{\beta,0}$ showed in Fig. 3. When these reference parameters will be changed, it will be specified in the text.

c. Results and discussion

The final HV is the pertinent parameter to analyze the results. According to Nebuloni (2005), it can be estimated by

$$\mathrm{HV} = \frac{3.91}{\beta_{\mathrm{ext}}(\lambda = 550\,\mathrm{nm})}, \quad \text{with} \tag{22}$$

$$\beta_{\mathrm{ext}} = \pi N_\alpha r_\alpha^2 Q_{\mathrm{ext}}(m, r_\alpha, \lambda), \tag{23}$$

where m is the refractive index, equal to the complex number $1.333–1.96 \times 10^{-9} i$ for pure water at a wavelength of 550 nm (Hale and Querry 1973). Figure 3 of Reuge et al. (2015) shows the extinction efficiency Q_{ext} calculated as a function of r_α.

For the first calculations (runs 1–15), only the coalescence induced by gravity is taken into account (i.e., $q_{r,\alpha\beta} = 0$). Operating conditions are given in Table 1. The coalescence induced by turbulence will be taken into account later.

TABLE 1. Operating conditions and results for runs 1–15 (run 1 is the reference; operating parameters that differ from those of run 1 are in boldface type).

Run	Salt	$d_{\beta,0}$ (μm)	$N_{\beta,\max}$ (cm^{-3})	$d_{\alpha,0}$ (μm)	$N_{\alpha,\max}$ (cm^{-3})	H_0 (m)	T (°C)	t_{tot}	EI (unitless)
1	NaCl	6.7	16	10	400	40	10	16 min 40 s	1
2	**KCl**	6.7	16	10	400	40	10	16 min 40 s	0.91
3	**$CaCl_2$**	6.7	16	10	400	40	10	16 min 40 s	0.89
4	NaCl	6.7	**22.5**	10	400	**75**	10	34 min	1.33
5	NaCl	6.7	**25**	10	400	**100**	10	45 min	1.60
6	NaCl	6.7	**29**	10	400	**150**	10	1 h 6 min	2.07
7[a]	NaCl	**5**	**22.5**	10	400	40	10	24 min 50 s	1.72
8	NaCl	**9**	**11**	10	400	40	10	11 min 40 s	0.60
9	NaCl	6.7	16	**8.7**	**600**	40	10	16 min 40 s	1
10	NaCl	6.7	**15**	**12.6**	**200**	40	10	16 min 40 s	1.05
11	NaCl	6.7	**9**	10	**200**	40	10	15 min 50 s	0.92
12	NaCl	6.7	**23**	10	**600**	40	10	18 min 20 s	1.05
13	NaCl	6.7	**18.5**	10	400	40	**5**	20 min	0.89
14	NaCl	6.7	**21**	10	400	40	**0**	23 min 20 s	0.73
15	NaCl	6.7 and **0.180**	16 and **160**	10	400	40	10	16 min 40 s	1

[a] Reuge et al. (2015).

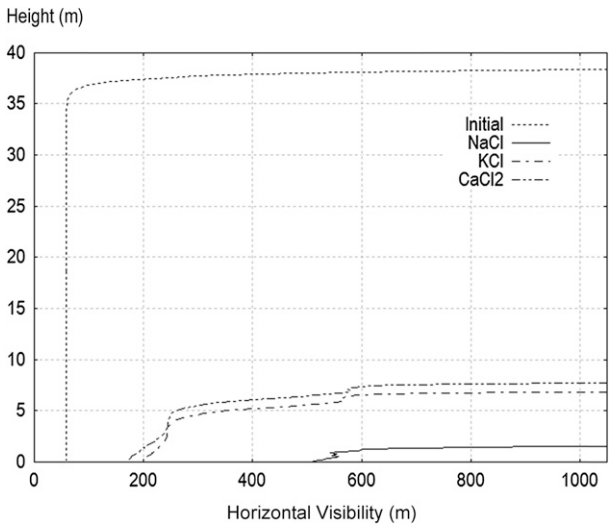

FIG. 4. Initial and final horizontal visibility vs height for runs 1, 2, and 3.

1) EFFECT OF THE CHOSEN SALT

According to section 3a, three salts are chosen to be tested: $CaCl_2$, NaCl, and KCl. For these first calculations (runs 1, 2, and 3), an initial value of $16\,cm^{-3}$ for the salted droplets' number density $N_{\beta,max}$ was considered. NaCl is used for run 1, KCl for run 2, and $CaCl_2$ for run 3 (Table 1).

The initial and final horizontal visibilities as a function of height are shown in Fig. 4. Using the salt NaCl, the fog layer is almost completely dissipated (i.e., horizontal visibility greater than 1000 m), but note that a thin fog layer of about 2-m height above the ground remains at the end of the process: a total dissipation would require a slightly higher value of $N_{\beta,max}$ ($16.8\,cm^{-3}$ instead of $16\,cm^{-3}$). Using the salts KCl or $CaCl_2$, only about 80% of the layer height is denebulized. KCl appears to be slightly more efficient than $CaCl_2$. Therefore, according to these results, the hygroscopicity of the salt at high dilution rates plays a key role (see section 3a). The denebulization processes last about 16 min 40 s for the three runs (Table 1). Calculations show that less than 0.4% of the fog droplets is captured by the salted droplets through coalescence induced by gravity. The denebulization process is mainly achieved by evaporation of the fog droplets and the concomitant condensation on the salted droplets.

Note that similar calculations have been performed with an initial diameter $d_{\alpha,0}$ of $9\,\mu m$ and a value of $11\,cm^{-3}$ for the salted droplets' number density $N_{\beta,max}$ in (Reuge et al. 2015) for the same salts. It led to almost identical results in terms of final horizontal visibilities but with a shorter total duration: 12 min 30 s (cf. Table 1 in Reuge et al. 2015).

Figure 5 shows the evolution of the fog droplet diameter d_α as a function of height and time for run 1. After an extremely rapid decrease of d_α in the zone where salt particles are seeded, it can be seen that the extent of the totally cleared zone ($d_\alpha = 0$) increases almost linearly as a function of time.

Figure 6 shows the evolution of the salted droplet diameter d_β as a function of height and time for run 1. For the sake of clarity, the diameters versus height curves at every given time have been drawn only where the salted droplets' number density N_β is greater than $N_{\beta,max}/10$. After an extremely rapid increase of d_β in the zone where the salt particles were seeded, the salted droplets fall more and more rapidly and the extent of their zone of presence increases with time, until they reach the ground.

Let us consider the following efficiency index (EI):

$$\mathrm{EI} = \frac{\text{Total mass of absorbed water/Mass of salt seeded}|_{\text{run } x}}{\text{Total mass of absorbed water/Mass of salt seeded}|_{\text{run } 1}}. \tag{24}$$

Run 1 is chosen as the reference run to define this efficiency index; therefore, EI(run 1) = 1. Then, the following values are obtained: EI(run 2) = 0.91 and EI(run 3) = 0.89.

Figure 7 shows the temporal evolution of the horizontal visibility at a height of 20 m. Between 200 and 400 s, more and more of the salted droplets cross this height, the fog droplets evaporate, and the HV increases. Between 430 and 520 s, the salted droplets' number density becomes so high that the HV decreases. Finally, after 520 s, the falling salted droplets' number density decreases to zero, leaving a layer of high visibility (>1000 m) after 550 s. Note that the small oscillations of the horizontal visibility shown in this figure are due to the oscillatory nature of the extinction efficiency Q_{ext} as a function of the droplet radius (see Fig. 3 of Reuge et al. 2015).

Then according to Fig. 8 (run 1), the final relative humidity in the layer has decreased significantly; RH is 99.3% toward the middle of the layer. Therefore, a part of the water absorbed by the salted droplets straightly comes from the initial ambient humidity. Close to the ground, RH remains 100% because the salted droplets have absorbed so much water during their fall that their

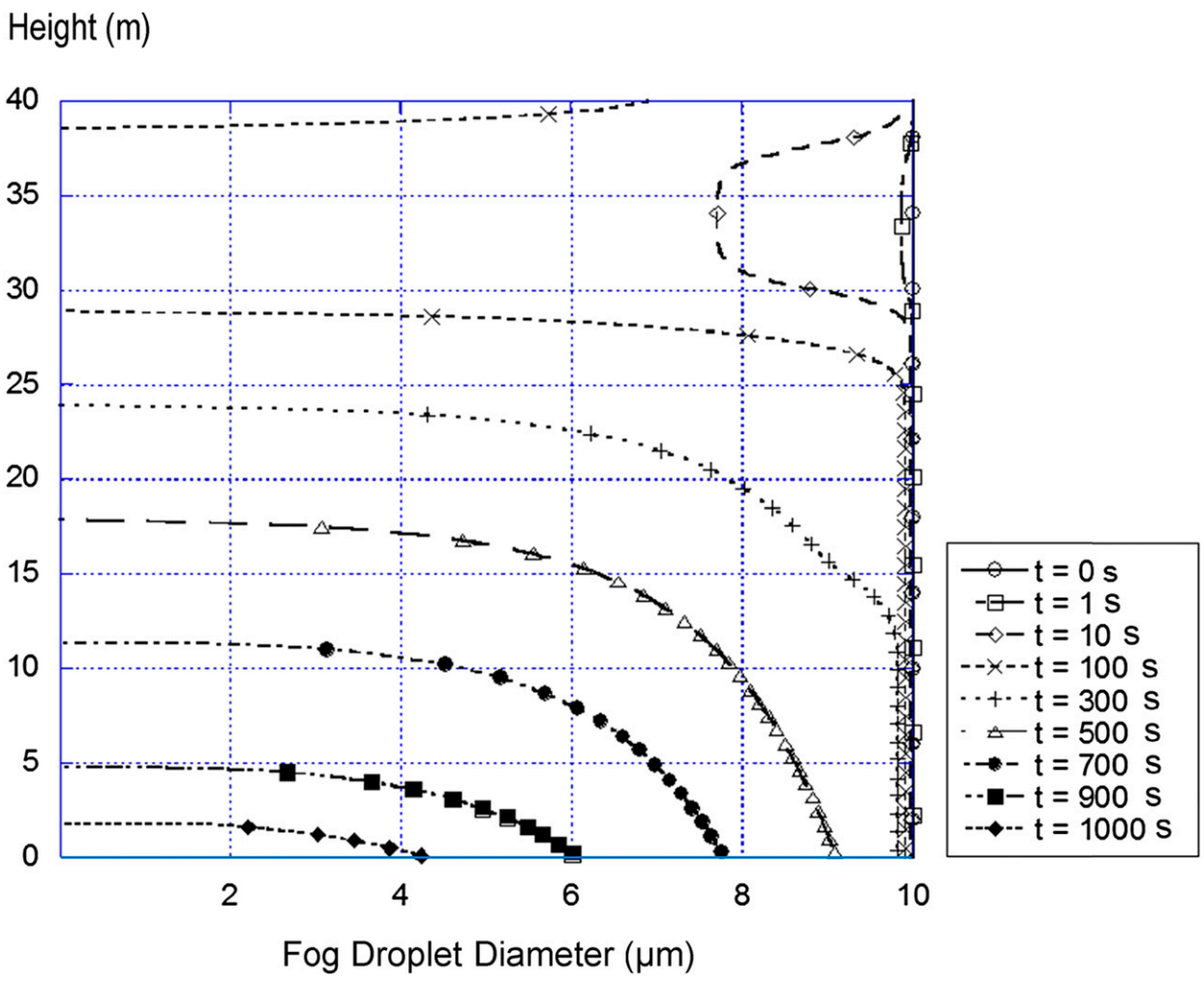

FIG. 5. Fog droplet diameter vs height and time for run 1.

salinity has become very low (i.e., the water activity in the solution is very close to 1); therefore, their ability to absorb water vapor has become insignificant. As already discussed in Reuge et al. (2015), a characteristic time of water vapor diffusion in air can be estimated (by L^2/D_v with $L = 20$ m), giving about 200 days. Therefore, the resaturation of the layer by water vapor (required for the formation of a new fog) will not be due to ordinary diffusion but rather to convection, turbulent diffusion, or temperature changes. This is a very interesting result.

Because NaCl is the more efficient salt in our operating conditions, it has been chosen for the following parts of this study.

2) EFFECT OF THE FOG-LAYER HEIGHT

Fog layers can vary from a few tens of centimeters to a few hundreds of meters. Three new calculations consider thicker fog layers (run 4: 75 m, run 5: 100 m, and run 6: 150 m). The values of the salted droplets' number density $N_{\beta,\max}$ have been adjusted to allow a complete denebulization of the fog (they are reported in Table 1 and Fig. 9). The $N_{\beta,\max}$ values have to be increased logically with the fog-layer thickness but not linearly because the thicker the fog layer, the longer the evaporation/condensation phenomena will take to proceed. This explains the increase of EI with the layer height (Table 1), reaching a value of 2 for the 150-m-height fog layer. A value of $N_{\beta,\max}$ of 25 cm^{-3} is required to denebulize the 100-m-height fog layer, and the time required is 45 min (Table 1 and Fig. 9).

Therefore, the higher the fog layer is, the more important is the required mass of salt to seed, and the longer the denebulization process lasts, but not linearly.

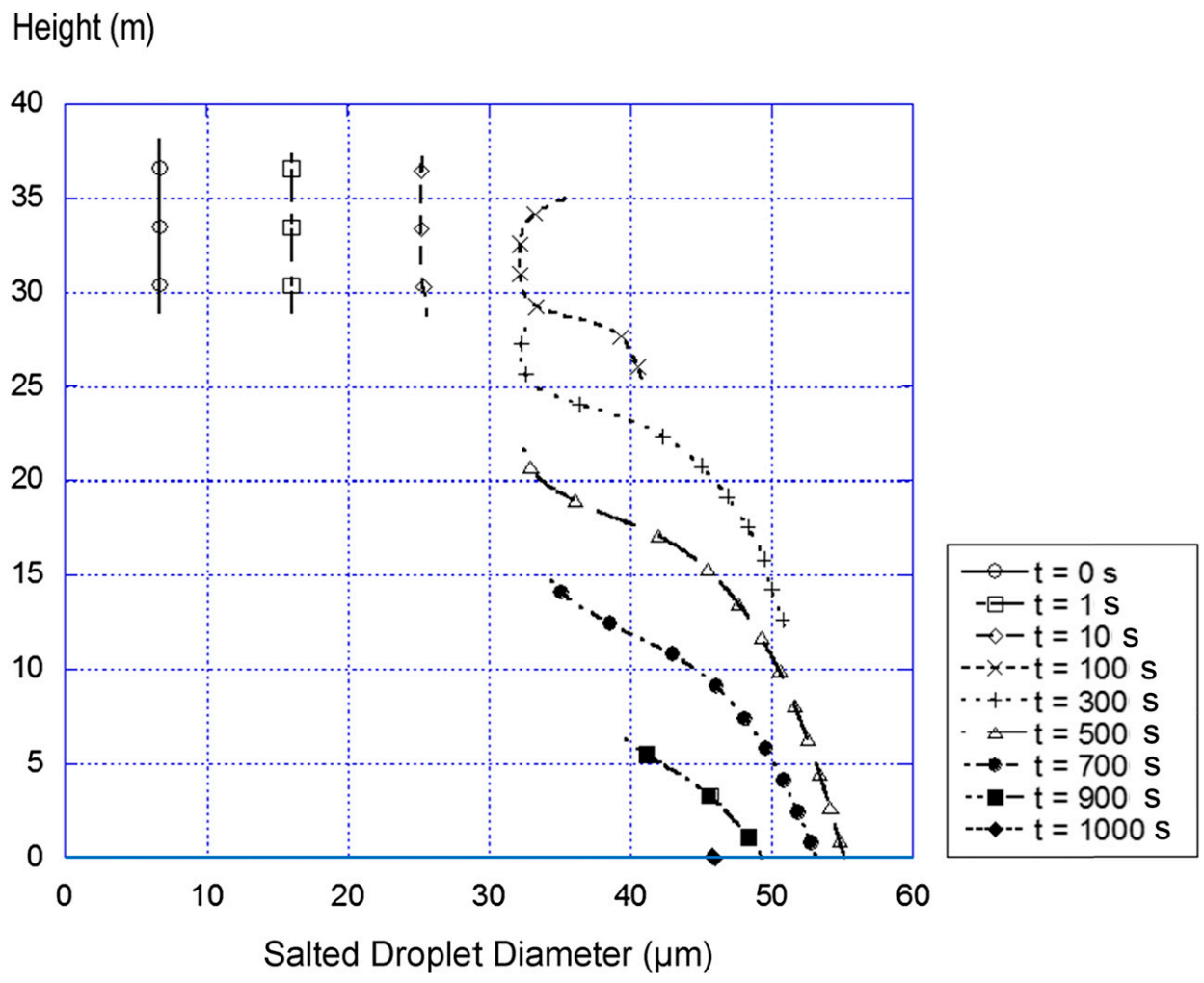

FIG. 6. Salted droplet diameter vs height and time for run 1.

3) EFFECT OF THE INITIAL DIAMETER OF THE SALT PARTICLES

Next, the effect of the initial seed particles diameter was investigated. Two additional runs have been performed using initial diameters of 5 μm (run 7; Reuge et al. 2015) and 9 μm (run 8). It appears that a value of the salted droplets' number density $N_{\beta,\max}$ of 22.5 particles per centimeter cubed is necessary for run 7 to denebulize the entire layer and 11 particles per centimeter cubed for run 8. The total mass of salt required increases with the initial particle diameter, as previously shown by Silverman and Kunkel (1970); this why EI is 1.72 for run 7 and only 0.60 for run 8 (Table 1). This can be explained simply: the smaller the initial particle diameters, the longer their fall lasts and the more time the salted droplets have to absorb the water. For run 7, the denebulization process lasts for 24 min 50 s, and only 11 min 40 s for run 8. Therefore, two opposing aspects must be considered for the choice of the initial particle diameter: the efficiency of the denebulization on one hand and its duration on the other hand.

4) EFFECT OF THE FOG PROPERTIES

As stated in section 3a, fog properties can vary, especially in terms of mean droplet diameter and droplet number density.

Two additional runs have been performed varying the initial fog droplets diameter and their number density N_α in such a way that the liquid water content in the layer remains constant in the layer (same as run 1). We considered $N_{\alpha,\max}$ of 600 cm^{-3} (run 9) and 200 cm^{-3} (run 10) with initial fog droplets diameters of 8.7 and 12.6 μm, respectively. As a result, the salt particles' number density required to dissipate the layer and EI remain almost the same (Table 1). Or, in other words, in this range of operating conditions, the total mass of seeded

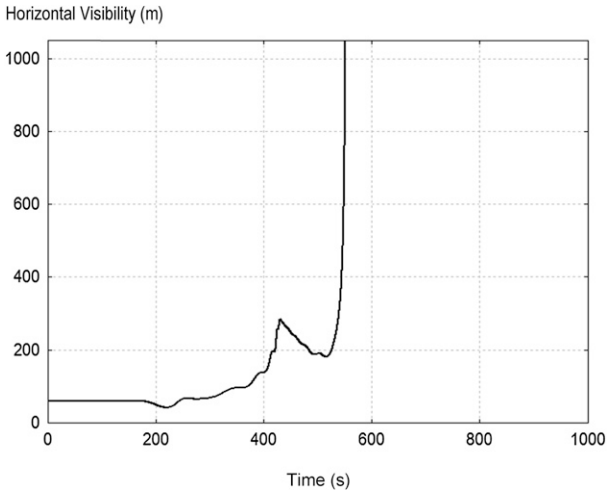

FIG. 7. Horizontal visibility vs time at a height of 20 m for run 1.

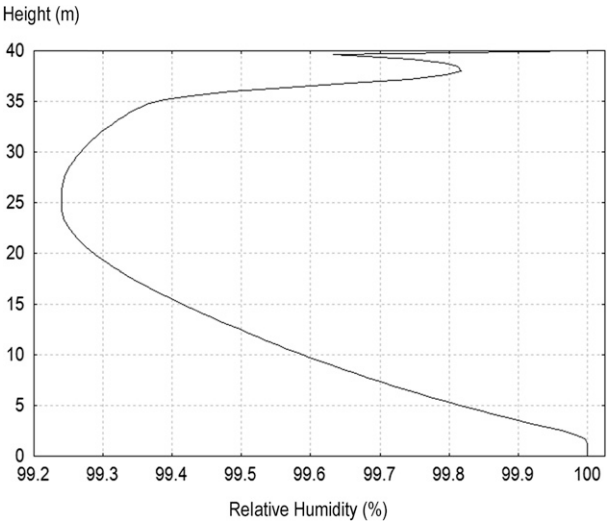

FIG. 8. Final relative humidity as a function of height for run 1.

particles required to dissipate the fog layer is proportional to the initial mass of liquid water in this fog layer. Durations do not change (16 min 40 s).

Then, two more runs were performed, keeping the initial fog droplets diameter of 10 μm but changing the fog droplets' number density $N_{\alpha,\max}$: first, 200 cm^{-3} (run 11) and then 600 cm^{-3} (run 12). The salted droplets' number density $N_{\beta,\max}$ must be 9 cm^{-3} to denebulize the layer (duration: 15 min 50 s) for run 11 and 23 cm^{-3} for run 12 (duration: 18 min 20 s). EI does not change significantly (0.92 for the first run; 1.05 for the second run) (Table 1).

Therefore, these results show that the salt particles' number density to seed to dissipate the layer is almost proportional to the initial mass of liquid water in the fog layer. This is in accordance with the results obtained by Silverman and Kunkel (1970) and Kuba and Murakami (2010).

5) EFFECT OF THE FOG TEMPERATURE

The effect of the fog temperature has been studied. Temperatures of 5° and 0°C have been considered for runs 13 and 14, respectively. Results are reported in Table 1. With a temperature of 0°C instead of 10°C, the number density of seed particles must be increased by 31% and the total time of denebulization is 1.4 times longer. Lower temperatures imply lower water vapor partial pressure in air P_{vap} and at the droplet surface P_{sat} and therefore slower evaporation–condensation phenomena. For this range of operating conditions, the salted droplets' number density $N_{\beta,\max}$ and the total time of denebulization t_{tot} required for a total denebulization of the layer increase almost linearly with the decrease of the temperature.

6) EFFECT OF THE PRESENCE OF SUBMICRONIC PARTICLES

To take into account the effect of the presence of submicronic seed particles in the plumes generated by the flares, a second class of particles has been added. This class 2 features particles of 180-nm diameter with a number density equal to 10 times the density of the supermicronic particles (class 1, 6.7-μm diameter). Thus, these submicronic particles only represent 0.02% of the total mass of the seed particles generated by the flares.

This new calculation (run 15) has been performed while keeping all other parameters identical to the reference run (run 1). The results show that these initially submicronic particles become salted droplet with a final diameter of about 1 μm. They remain too small to fall to the ground and actually generate an artificial "salted mist" at the top of the initial fog layer. Figure 10 compares the final horizontal visibility for runs 1 and 15: this additional mist is clearly insignificant; the final horizontal visibility remains greater than 1000 m. Therefore, for these operating conditions, the presence of submicronic particles is not problematic.

7) EFFECT OF THE TURBULENCE INTENSITY

Turbulence intensity is much lower in fogs than in clouds. However, it can vary significantly according to the type of fog and the wind velocity. Finally, three new calculations have been performed, taking the turbulence-induced coalescence into account. Runs 17, 18, and 19 consider turbulence kinetic energies k of 0.1, 0.3, and 1 $m^2 s^{-2}$, respectively, and dissipation rates of turbulence kinetic energy ε of 10, 30, and 100 $cm^2 s^{-3}$, respectively.

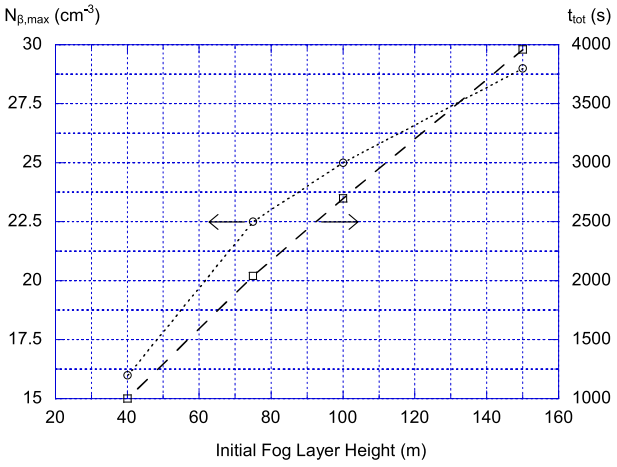

FIG. 9. Seed particle density $N_{\beta,\max}$ (dotted) and total time of denebulization t_{tot} (dashed) as a function of initial fog-layer height.

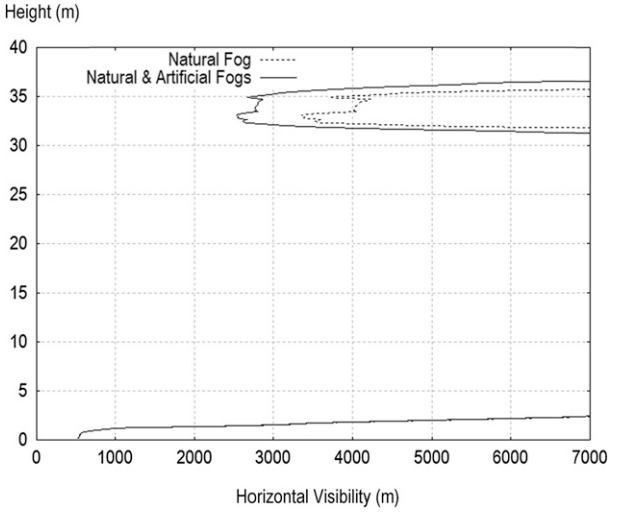

FIG. 10. Final horizontal visibility vs height for runs 1 and 15.

The fog-layer height has been fixed to 60 m and a value of only 12 particles per centimeter cubed has been applied for $N_{\beta,\max}$. A new reference case (run 16) has been performed in these conditions without turbulence: the fog layer is dissipated over about 20 m only (toward the top of the layer). Table 2 shows the ratio $\Delta N_\alpha/N_{\alpha,0}$ given by the following expression:

$$\frac{\Delta N_\alpha}{N_{\alpha,0}} = \frac{\int_0^H (N_{\alpha,f} - N_{\alpha,0})\, dz}{\int_0^H N_{\alpha,0}\, dz}. \tag{25}$$

For run 16, $\Delta N_\alpha/N_{\alpha,0}$ is -0.42% (Table 2). In a typical fog, it appears that the coalescence induced by turbulence is the same order of magnitude as the coalescence induced by gravity (run 17; Table 2); $\Delta N_\alpha/N_{\alpha,0}$ is -1%. In the most favorable case (run 19), $\Delta N_\alpha/N_{\alpha,0}$ reaches -3.1%. The effect of the turbulence is too small to significantly promote coalescence and to affect the final horizontal visibility. Therefore, in our operating conditions, the effect of the turbulence intensity is insignificant.

4. Conclusions

A model including mass transfers (condensation/evaporation) and gravity-induced and turbulence-induced coalescence has been used to model the time evolution of a warm fog made of pure water droplets and hygroscopic particles. The model allows us to analyze the effect of salt compositions in changing the hygroscopic efficiency of the salted droplets.

Among the three salts considered in this study (NaCl, KCl, and $CaCl_2$), NaCl is the most efficient for denebulizing a typical warm fog because of its highest hygroscopicity at high dilution rates. In our operating conditions, the dissipation of the fog is mainly due to evaporation/condensation phenomena. Coalescence induced by gravity and by turbulence is negligible and has no significant effect on the final horizontal visibility. These results differ from those of Silverman and Kunkel (1970): their calculations showed a significant role played by the coalescence induced by gravity because they considered a fog initially formed of much bigger droplets and much thicker layers. Their results and the results presented here are not comparable because the operating conditions differ, but they are complementary.

The efficiency of the denebulization increases as the initial particle diameter decreases. The larger the initial particle diameter, the higher the necessary mass of the seed to dissipate the fog. However, the duration of the denebulization process decreases as the initial particle diameter increases. Therefore, two opposing aspects must be considered for the choice of the initial particle diameter: the efficiency of the denebulization on one hand and its duration on the other hand. An initial particle diameter of 6.7 μm seems to be a good compromise in our operating conditions. Moreover, calculations have shown that the mass required to denebulize the fog layer

TABLE 2. Operating conditions and results for runs 16–19.

Run	$N_{\beta,\max}$ (cm^{-3})	H_0 (m)	k ($m^2\,s^{-2}$)	ε ($cm^2\,s^{-3}$)	$\Delta N_\alpha/N_{\alpha,0}$ (%)
16	12	60	—	—	−0.42
17	12	60	0.1	10	−1.01
18	12	60	0.3	30	−1.70
19	12	60	1	100	−3.1

of a given height is almost proportional to the initial quantity of the liquid water in this layer.

An a priori unexpected result is that the salted droplets absorb the water not only from the fog droplets but also from the ambient humidity. Thus, a new fog cannot reform immediately after the end of the process, at least as long as the air is not resaturated with water vapor.

The higher the fog temperature, the more efficient the denebulization process. The required mass of salt particles to seed increases almost linearly as the temperature decreases.

The presence of initially submicronic particles in the plumes generated by the flare does not seem to impact the efficiency of the process in our operating conditions.

From the calculations, 15 kg of NaCl seed microparticles can dissipate a fog layer of 40-m height over 0.25 km^2 in less than 17 min. This is suitable for the targeted application.

The technique requires an appropriate anticipation in the treatment: first, the main properties of the fog (liquid water content, mean droplet diameter, temperature) and the velocity and the direction of the wind must be measured. Then, according to the thickness of the layer that must be denebulized, a specific amount of salt particles must be seeded in a specific area to achieve the goal at the wanted location and timing. The first experiments on site are leading to very promising results.

Acknowledgments. We acknowledge Bpifrance for funding this research project and Frédéric Burnet from Météo France for helpful discussions.

APPENDIX

Definition of Terms

a. Variables

$a_{w,\beta}$	Water activity in the solution (unitless)
d	Diameter (m)
D_v	Diffusion coefficient of water vapor in air ($m^2 s^{-1}$)
E_{coll}	Collision efficiency (unitless)
E_{coal}	Coalescence efficiency (unitless)
$F_{\alpha\beta}$	Coalescence frequency between droplets α/β ($m^{-3} s^{-1}$)
g	Standard gravity acceleration ($m s^{-2}$)
$g_{r,\alpha\beta}$	Mean relative velocity between droplets of phase α and droplets of phase β ($m s^{-1}$)
HV	Horizontal visibility (m)
EI	Efficiency index (unitless)
k	Turbulence kinetic energy ($m^2 s^{-2}$)
m	Water refractive index (unitless)
M	Molar mass (kg mol^{-1})
N	Number density (m^{-3})
P_{vap}	Water vapor partial pressure (Pa)
P_s	Saturation water vapor partial pressure at the salted droplet surface (Pa)
P_{sat}	Saturation water vapor partial pressure in air (Pa)
q_k^2	Agitation of the droplets of phase k ($m^2 s^{-2}$)
Q_{ext}	Extinction efficiency (unitless)
R	Gas constant (J $mol^{-1} K^{-1}$)
r_α	Fog droplet radius (m)
R_β	Seed particle–salted droplet radius (m)
RH	Relative humidity (%)
Sh	Sherwood number (unitless)
t	Time (s)
t_{tot}	Total time of denebulization (s)
T	Temperature (K)
v	Terminal settling velocity ($m s^{-1}$)
z	Vertical coordinate (m)

b. Greek

$\Gamma_{\alpha\beta}$	Radial distribution function (unitless)
β_{ext}	Extinction coefficient (m^{-1})
ε	Dissipation rate of the turbulence kinetic energy ($m^2 s^{-3}$)
ε_k	Volume fraction for phase k (unitless)
λ	Wavelength (m)
λ_m	Mean free path (m)
μ	Dynamic viscosity (Pa s)
η_t	Inverse of the Stokes number (unitless)
ρ	Density ($kg m^{-3}$)
τ_f	Lagrangian turbulent time scale (s)
τ_p	Particle response time scale (s)

c. Subscript

0	Initial
a	Air
α	Fog droplet phase
β	Seed particle/droplet phase
k	Liquid phase index (α or β)
w	Liquid water

REFERENCES

Beard, K. V., and H. T. Ochs, 1995: Collisions between small precipitation drops. Part II: Formulas for coalescence, temporary coalescence, and satellites. *J. Atmos. Sci.*, **52**, 3977–3996, doi:10.1175/1520-0469(1995)052<3977:CBSPDP>2.0.CO;2.

Cooper, W. A., and R. T. Bruintjes, 1997: Calculations pertaining to hygroscopic seeding with flares. *J. Appl. Meteor.*, **36**, 1449–1469, doi:10.1175/1520-0450(1997)036<1449:CPTHSW>2.0.CO;2.

Csanady, G., 1963: Turbulent diffusion of heavy particles in the atmosphere. *J. Atmos. Sci.*, **20**, 201–208, doi:10.1175/1520-0469(1963)020<0201:TDOHPI>2.0.CO;2.

Cunningham, E., 1910: On the velocity of steady fall of spherical particles through fluid medium. *Proc. Roy. Soc. London*, **83A**, 357–365, doi:10.1098/rspa.1910.0024.

Dupont, J.-C., M. Haeffelin, A. Protat, D. Bouniol, N. Boyouk, and Y. Morille, 2012: Stratus fog formation and dissipation: A 6-day case study. *Bound.-Layer Meteor.*, **143**, 207–225, doi:10.1007/s10546-012-9699-4.

Gourdel, C., O. Simonin, and E. Brunier, 1999: Two-Maxwellian equilibrium distribution function for the modelling of a binary mixture of particles. *Circulating Fluidized Bed Technology VI: Proceedings of the 6th International Conference on Circulating Fluidized Beds*, J. Werther, Ed., DECHEMA, 205–210.

Hale, G. M., and M. R. Querry, 1973: Optical constants of water in the 200-nm to 200-μm wavelength region. *Appl. Opt.*, **12**, 555–563, doi:10.1364/AO.12.000555.

Hamer, W. J., and Y.-C. Wu, 1972: Osmotic coefficients and mean activity coefficients of uni-univalent electrolytes in water at 25°C. *J. Phys. Chem. Ref. Data*, **1**, 1047–1100, doi:10.1063/1.3253108.

Han, S., Z. Cai, Y. Zhang, J. Wang, Q. Yao, P. Li, and X. Li, 2015: Long-term trends in fog and boundary layer characteristics in Tianjin, China. *Particuology*, **20**, 61–68, doi:10.1016/j.partic.2014.02.008.

Hinds, W. C., 1982: *Aerosol Technology: Properties, Behavior, and Measurement of Airborne Particles.* John Wiley & Sons, 424 pp.

Jiusto, J. E., R. J. Pilié, and W. C. Kocmond, 1968: Fog modification with giant hygroscopic nuclei. *J. Appl. Meteor.*, **7**, 860–869, doi:10.1175/1520-0450(1968)007<0860:FMWGHN>2.0.CO;2.

Koening, L. R., 1971: Numerical experiments pertaining to warm-fog clearing. *Mon. Wea. Rev.*, **99**, 227–241, doi:10.1175/1520-0493(1971)099<0227:NEPTWC>2.3.CO;2.

Kornfeld, P., 1970: Some numerical experiments for warm fog clearing by seeding with hygroscopic nuclei. *J. Appl. Meteor.*, **9**, 459–463, doi:10.1175/1520-0450(1970)009<0459:SNEFWF>2.0.CO;2.

Kruis, F. E., and K. A. Kusters, 1997: The collision rate of particles in turbulent flow. *Chem. Eng. Commun.*, **158**, 201–230, doi:10.1080/00986449708936589.

Kuba, N., and M. Murakami, 2010: Effect of hygroscopic seeding on warm rain clouds—Numerical study using a hybrid cloud microphysical model. *Atmos. Chem. Phys.*, **10**, 3335–3351, doi:10.5194/acp-10-3335-2010.

Kunkel, B. A., and B. A. Silverman, 1970: A comparison of the warm fog clearing capabilities of some hygroscopic materials. *J. Appl. Meteor.*, **9**, 634–638, doi:10.1175/1520-0450(1970)009<0634:ACOTWF>2.0.CO;2.

Liu, D., J. Yang, S. Niu, and Z. Li, 2011: On the evolution and structure of a radiation fog event in Nanjing. *Adv. Atmos. Sci.*, **28**, 223–237, doi:10.1007/s00376-010-0017-0.

Mather, G. K., D. E. Terblanche, F. E. Steffens, and L. Fletcher, 1997: Results of South African cloud seeding experiments using hygroscopic flares. *J. Appl. Meteor.*, **36**, 1433–1447, doi:10.1175/1520-0450(1997)036<1433:ROTSAC>2.0.CO;2.

Nebuloni, R., 2005: Empirical relationships between extinction coefficient and visibility in fog. *Appl. Opt.*, **44**, 3795–3804, doi:10.1364/AO.44.003795.

Pigeonneau, F., 1998: Modélisation numérique des collisions de gouttes en écoulements laminaires et turbulents. Ph.D. thesis, Université Paris VI, 229 pp.

Pinsky, M., A. Khain, and M. Shapiro, 2001: Collision efficiency of drops in a wide range of Reynolds numbers: Effects of pressure on spectrum evolution. *J. Atmos. Sci.*, **58**, 742–764, doi:10.1175/1520-0469(2001)058<0742:CEODIA>2.0.CO;2.

Rard, A. R., and S. L. Clegg, 1997: Critical evaluation of the thermodynamic properties of aqueous calcium chloride. 1. Osmotic and activity coefficients of 0–10.77 mol kg^{-1} aqueous calcium chloride solutions at 298.15 K and correlation with extended Pitzer ion-interaction models. *J. Chem. Eng. Data*, **42**, 819–849, doi:10.1021/je9700582.

Reid, R. C., J. M. Prausnitz, and T. K. Sherwood, 1977: *The Properties of Gases and Liquids*. 3rd ed. McGraw-Hill, 688 pp.

Reuge, N., J. Dexpert-Ghys, M. Verelst, and B. Caussat, 2008: Y_2O_3:Eu micronic particles synthesised by spray pyrolysis: Global modelling and optimisation of the evaporation stage. *Chem. Eng. Process.*, **47**, 731–743, doi:10.1016/j.cep.2006.12.007.

——, P. Fede, J.-F. Berthoumieu, F. Foucoin, and O. Simonin, 2015: 1-D modeling of the denebulization of fogs by hygroscopic seeding. *Proc. ASME/JSME/KSME 2015 Joint Fluids Engineering Conf./14th Int. Symp. on Gas-Liquid Two-Phase Flows*, Seoul, South Korea, Fluids Engineering Division, 5 pp., doi:10.1115/AJKFluids2015-30188.

Schaefer, V., 1946: The production of ice crystals in a cloud of supercooled water droplets. *Science*, **104**, 457–459, doi:10.1126/science.104.2707.457.

Segal, Y., A. Khain, M. Pinsky, and D. Rosenfeld, 2004: Effects of hygroscopic seeding on raindrop formation as seen from simulations using a 2000-bin spectral cloud parcel model. *Atmos. Res.*, **71**, 3–34, doi:10.1016/j.atmosres.2004.03.003.

Silverman, B. A., and B. A. Kunkel, 1970: A numerical model of warm fog dissipation by hygroscopic particle seeding. *J. Appl. Meteor.*, **9**, 627–633, doi:10.1175/1520-0450(1970)009<0627:ANMOWF>2.0.CO;2.

Van Hop, H., Ed., 1989: *Air Pollution Modeling and its Application VII*. Nato Challenges of Modern Society, Vol. 7, Springer, 620 pp.

Yudine, M., 1959: Physical consideration on heavy-particle dispersion. *Advances in Geophysics*, Vol. 6, Academic Press, 185–191, doi:10.1016/S0065-2687(08)60106-5.

Zaichik, L. I., P. Fede, O. Simonin, and V. M. Alipchenkov, 2009: Statistical models for predicting the effect of bidisperse particle collisions on particle velocities and stresses in homogeneous anisotropic turbulent flows. *Int. J. Multiphase Flow*, **35**, 868–878, doi:10.1016/j.ijmultiphaseflow.2009.05.007.